Available online at www.sciencedirect.com

ScienceDirect

Advances in Space Research 61 (2018) 2569–2584

ADVANCES IN SPACE RESEARCH (a COSPAR publication)

www.elsevier.com/locate/asr

A comparative study of ionospheric IRIEup and ISP assimilative models during some intense and severe geomagnetic storms

M. Pietrella [a,*], A. Pignalberi [b], M. Pezzopane [a], A. Pignatelli [a], A. Azzarone [a], R. Rizzi [b]

[a] *Istituto Nazionale di Geofisica e Vulcanologia, 00143 Rome, Italy*
[b] *Department of Physics and Astronomy, University of Bologna, Bologna, Italy*

Received 7 November 2017; received in revised form 19 February 2018; accepted 20 February 2018
Available online 2 March 2018

Abstract

Three-dimensional (3-D) electron density matrices, computed in the Mediterranean area by the *IRI* climatological model and *IRIEup* and *ISP* nowcasting models, during some intense and severe geomagnetic-ionospheric storms, were ingested by the ray tracing software tool IONORT, to synthesize quasi-vertical ionograms. *IRIEup* model was run in different operational modes: (1) assimilating validated autoscaled electron density profiles only from a limited area which, in our case, is the Mediterranean sector (*IRIEup_re(V)* mode); (2) assimilating electron density profiles from a larger region including several stations spread across Europe: (a) without taking care of validating the autoscaled data in the assimilation process (*IRIEup(NV)*); (b) validating carefully the autoscaled electron density profiles before their assimilation (*IRIEup(V)*).

The comparative analysis was carried out comparing *IRI*, *IRIEup_re(V)*, *ISP*, *IRIEup(NV)*, and *IRIEup(V)* *fo*F2 synthesized values, with corresponding *fo*F2 measurements autoscaled by ARTIST, and then validated, at the truth sites of Roquetes (40.80°N, 0.50°E, Spain), San Vito (40.60°N, 17.80°E, Italy), Athens (38.00°N, 23.50°E, Greece), and Nicosia, (35.03°N, 33.16°E, Cyprus). The outcomes demonstrate that: (1) *IRIEup_re(V)*, performs better than *ISP* in the western Mediterranean (around Roquetes); (2) *ISP* performs slightly better than *IRIEup_re(V)* in the central part of Mediterranean (around Athens and San Vito); (3) *ISP* performance is better than the *IRIEup_re(V)* one in the eastern Mediterranean (around Nicosia); (4) *IRIEup(NV)* performance is worse than the *IRIEup(V)* one; (5) in the central Mediterranean area, *IRIEup(V)* performance is better than the *IRIEup_re(V)* one, and it is practically the same for the western and eastern sectors.

Concerning the overall performance, nowcasting models proved to be considerably more reliable than the climatological *IRI* model to represent the ionosphere behaviour during geomagnetic-ionospheric storm conditions; *ISP* and *IRIEup(V)* provided the best performance, but neither of them has clearly prevailed over the other one.

Keywords: (3-D) electron density mapping; IRI model; IRIEup model; ISP model; Ionospheric ray tracing; Simulated quasi vertical ionograms

1. Introduction

The expression "Space Weather" is usually meant to describe the physical conditions characterizing the near-Earth space including the ionosphere and the magnetosphere. Such conditions can be significantly perturbed essentially because of important events occurring on the Sun, as coronal mass ejections and solar flares which, in turn, considerably affect the solar wind. A wide variety of physical phenomena, including geomagnetic storms and sub-storms, ionospheric perturbations, geomagnetically induced electric currents at the Earth's surface, are associated to Space Weather. They usually have a deep impact on the human life and technological systems. Malfunctions of over-the-horizon (OTH) radars and navigation systems

* Corresponding author.
E-mail address: marco.pietrella@ingv.it (M. Pietrella).

https://doi.org/10.1016/j.asr.2018.02.026
0273-1177/

based on Global Positioning System (GPS) satellites, serious damages to satellites, power distribution network, increased corrosion of pipelines, and the disrupt of radio communications, can be directly attributed to particular Space Weather conditions (Moldwin, 2008).

Given the growing societal dependence on technological systems, the real time near-Earth space environment conditions monitoring has become more and more important over the years, to forecast and nowcast the adverse effects caused by large Space Weather events (see the portal http://swe.ssa.esa.int/web/).

In particular, to mitigate the adverse Space Weather effects on the ionosphere, the development of models that, after assimilating real time measurements, provide full three-dimensional (3-D) electron density matrices has become increasingly important. To pursue this aim, some ionospheric models based on different assimilative techniques have been recently proposed:

(a) the data assimilation model called Global Assimilation of Ionospheric Measurements (GAIM), developed by Schunk et al. (2004), uses a physics-based ionosphere-plasmasphere model and a Kalman filter to assimilate a diverse set of real-time observations, providing a time dependent specification of the 3-D electron density distribution on a spatial grid that can be global, regional, or local;
(b) the Global Assimilative Ionospheric Model (GAIM) utilizes data assimilation techniques, to nowcast the Earth's ionosphere. It has proved to be effective in providing a better comprehensive specification of the ionosphere, improving the estimation of the electron density profile over the climatological model after assimilating ground GPS total electron content (TEC) measurements (Wang et al., 2004);
(c) the Electron Density Assimilative Model (EDAM) uses observations of slant TEC, as well as radio occultation data from the COSMIC satellite constellation, to adjust the ionospheric background calculated with the Parameterised Ionospheric Model (PIM) (Daniell et al., 1995), to get a near real time empirical 3-D distribution of the ionospheric electron density (Angling and Khattatov, 2006; Buresova et al., 2009);
(d) IonoNumerics is a numerical global model of the ionosphere which, even if does not utilize any climatological information, it provides real time electron density grids through the integration of a set of time-dependent differential equations describing the conservation of mass, momentum and energy (Bailey and Balan, 1996; Fuller-Rowell et al., 1996; Millward et al., 1996), and the use of measured slant TEC from a network of ground-based GPS receivers (Angling and Khattatov, 2006);
(e) the NeQuick2 model, which is an updated version of NeQuick (Hochegger et al., 2000; Radicella and Leitinger, 2001), is another global assimilative model that, ingesting experimental data, usually GPS-derived TEC and/or ionosonde-derived ionospheric peak parameters values, provides a 3-D specification of the electron density of the ionosphere for given epochs and geographic areas where experimental data are available (Nava et al., 2011);
(f) the IRI Real Time Assimilative Model (IRTAM) (Galkin et al., 2012) uses the underlying empirical quiet-time International Reference Ionosphere (*IRI*) representation of the ionosphere (Bilitza, 2001; Bilitza and Reinisch, 2008; Bilitza et al., 2014, 2017) to constrain the process of its elastic transformation into a better match with observations. The underlying *IRI* representation ensures that, when and where the measurements are not available, the assimilative model keeps its updates compatible with the empirical knowledge of the system. IRTAM uses a 24-h window of the deviations to adjust the original coefficients of the diurnal/spatial *IRI* expansion, and a low-pass temporal filter as a part of its diurnal harmonics analysis to smooth out data jitter, outliers, and low-confidence values.

The IRI-SIRMUP-P (*ISP*) and *IRIEup* are the two models developed at the Istituto Nazionale di Geofisica and Vulcanologia (INGV), with the support of the University of Bologna as far as the *IRIEup* model is concerned (Pezzopane et al., 2011, 2013; Pignalberi et al., 2018a,b).

The *ISP* model is a regional model able to provide a 3-D real time imaging of the ionosphere over the Mediterranean area. It is based on the ingestion of the F2-layer critical frequency *fo*F2 and propagation factor *M*(3000)F2 values, and the assimilation of observed electron density profiles from some reference stations. Specifically, for this study the ionospheric working stations located in the Mediterranean area, El Arenosillo (37.10°N, 6.70°W, Spain), Roquetes (40.80°N, 0.50°E, Spain), Rome (41.80°N, 12.50°E, Italy), Gibilmanna (37.90°N, 14.00°E, Italy), San Vito (40.60°N, 17.80°E, Italy), Athens (38.00°N, 23.50°E, Greece), and Nicosia (35.03°N, 33.16°E, Cyprus), have been employed sometimes as reference stations and sometimes as truth sites, as it will be clarified in Section 3.

At first, *ISP* outputs a 3-D updated matrix of the electron density generated combining the *IRI* model with the Simplified Ionospheric Regional Model Updated (SIRMUP) (Zolesi et al., 2004; Tsagouri et al., 2005) and, subsequently, an assimilation process of measured electron density profiles from the reference stations further updates the IRI-SIRMUP electron density profiles, thus generating an *ISP* 3-D matrix (Pezzopane et al., 2011, 2013).

The *IRIEup* model also relies on *IRI*, but not on SIRMUP, and hence it has the potentiality to operate on a global scale. In this work we refer to it as *IRIEup* because we applied it over the European sector. Analogously to *ISP*

model, *IRIEup* is based on a two steps method: firstly, after assimilating measured *fo*F2 and *M*(3000)F2 values, it updates the *IRI* background by means of effective ionospheric/solar indices maps (*IRI UP* method, Pignalberi et al., 2018a,b); secondly, it further updates the output implementing a technique, different from the *ISP* one, to assimilate the measured electron density profiles, thus providing a 3-D specification of the ionosphere.

In this paper the behaviour of *IRIEup* and *ISP* is compared for some very disturbed epochs included in recent geomagnetic-ionospheric storms occurred in March and December 2015, and October 2016.

In principle, as the comparison between the two models must be coherent as far as possible, *IRIEup* and *ISP* must operate under the same conditions. This means that they have to assimilate validated measured electron density profiles from the same reference stations. For these reasons, *IRIEup* is applied over the same *ISP* model validity area, i.e., over a limited area which, in our case, is the Mediterranean one; to this operational mode we refer hereafter as *IRIEup_re(V)* ("*re*" stands for "restricted area", and *(V)* means that before the assimilation the autoscaled ionograms were validated).

Nevertheless, the behaviour of the *IRIEup* model was also investigated under two other different operative modes, namely assimilating electron density profiles from a larger region including several stations spread across Europe: (a) without taking care of validating the autoscaled data before the assimilation process; (b) validating carefully the autoscaled data before their assimilation. To these two additional operational modes we refer hereafter as *IRIEup(NV)* (*(NV)* stands for "not validated") and *IRIEup(V)* respectively.

Moreover, we have also considered the *IRI* model alone (the *IRI* 2016 was used throughout the analysis in this paper), to investigate whether the *IRIEup* and *ISP* assimilation techniques can output better ionospheric predictions than *IRI* ones.

As the models output numerical grids representing 3-D electron density mappings of the ionosphere over a relatively large area, we thought to use these grids as the ionospheric environment to calculate synthesized ionograms by a ray tracing program. In the past, Angling and Khattatov (2006) considering the Segmented Method of Analytical Ray Tracing (SMART) (Norman and Cannon, 1997), synthesized oblique ionograms using the electron density grids provided by EDAM and IonoNumerics; the simulated corresponding maximum usable frequencies (MUFs) were then compared with measured MUFs over the oblique radio sounding between Inskip (53.50°N, 2.50°W, United Kingdom) and Rome (41.80°N, 12.50°E, Italy) to evaluate the goodness of both models.

Oblique-incidence radiosounding measurements are not available for the disturbed periods under investigation, thus we could not adopt the procedure followed by Angling and Khattatov (2006).

Nevertheless, the 3-D *IRI*, *IRIEup_re(V)*, *ISP*, *IRIEup (NV)*, and *IRIEup(V)* electron density distributions were ingested by the software tool named IONORT (IONOspheric Ray Tracing), (Azzarone et al., 2012), to synthesize quasi vertical ionograms at the truth sites specified in Section 3.

It is important to point out that the *IRI* model was run with the STORM option "ON" (Fuller-Rowell et al., 1998; Araujo-Pradere et al., 2002), in order to model at best the intense and severe geomagnetic-ionospheric storms considered in this investigation.

The *IRI*, *IRIEup_re(V)*, *ISP*, *IRIEup(NV)*, and *IRIEup (V)* *fo*F2 synthesized values were then compared with the corresponding *fo*F2 measurements autoscaled at the truth sites, by the Automatic Real-Time Ionogram Scaler with True height analysis (ARTIST) system (Reinisch and Huang, 1983; Reinisch et al., 2005; Bamford et al., 2008; Galkin and Reinisch, 2008; Stankov et al., 2012), to evaluate the goodness of models.

Since the *ISP* model was widely described and tested in the past, its description is omitted here, the interested reader can refer to the existing literature (Pezzopane et al. 2011, 2013) to get more details on how this model works. Conversely, the *IRIEup* model is a new assimilative model which has not been yet published. For this reason, a short description of it is provided in Section 2. The data analysis and results are presented in Section 3. The corresponding discussion is given in Section 4, while a short summary is the subject of Section 5.

2. The IRIEup assimilation algorithm: a short description

The *IRIEup* method is characterized by a first step through which measurements of *fo*F2 and *M*(3000)F2 carried out at each station are assimilated, to calculate effective values of the 12-months smoothed ionospheric index IG_{12} (derived by the IG index as calculated by Liu et al., 1983), and effective values of the 12-months smoothed sunspots number R_{12}, that is IG_{12eff} and R_{12eff} (Houminer et al. 1993; Pignalberi et al., 2018a,b).

From the scattered values of IG_{12eff} and R_{12eff}, corresponding maps are generated by means of the universal Kriging geostatistical interpolation method (Kitanidis, 1997). Then, these maps are used as input to the *IRI* model, obtaining a 3-D updated representation of the electron density identified as B_{ijk}, where: $i = 1, \ldots, nlon$ is the index of longitudes, being *nlon* the grid point number running on the *x*-axis; $j = 1, \ldots, nlat$ is the index of latitudes, being *nlat* the grid point number running on the *y*-axis; $k = 1, \ldots, nheight$ is the index of heights, being *nheight* the grid point number running on the *z*-axis.

The matrix B_{ijk} consists of $nlon \cdot nlat$ that is $i \cdot j$ one-dimensional updated *IRI* vertical electron density profiles b_k.

To better describe the *IRIEup* assimilation algorithm, the following mathematical notation is used: the geometric

dimension of each entity used in the algorithm is described by the number of subscript indices to the left of comma, while the mathematical product of the number of elements to the right of comma represents the number of these entities. For example, with this notation, the $nlon \cdot nlat$ one-dimensional vertical electron density profiles b_k can be expressed as $b_{k,ij}$; the single index k to the left of comma means that the entity b is a one-dimensional vector whose values depend on the height, the product of the number of elements of the two indices to the right of comma $i \cdot j$ means that we have $nlon \cdot nlat$ vectors b_k.

B_{ijk} is instead a 3-D matrix function of longitude, latitude and height. B_{ijk} can be also considered as k bi-dimensional matrices B_{ij}, thus, with the aforementioned notation, it can be written as $B_{ij,k}$. The $B_{ij,k}$ matrix will be our background reference state.

Let us assume to have *nstation* vertical radio-sounding ionospheric stations, described by the index $l = 1, \ldots, nstation$, whose longitude and latitude are respectively $X_{,l}$ and $Y_{,l}$ (there are *nstation* scalar values of longitude and latitude, and consequently there is no index to the left of comma). Vertical electron density profiles provided by the reference ionospheric stations, that will be used in the assimilation process, are identified as $I_{k,l}$.

The idea is to spread the information of each assimilated vertical profile on every grid point (i, j, k), with a weight inversely proportional to the distance between the assimilated profile location and the grid point. To accomplish this task, several *Radial Basis Functions* can be used as weighting function. Our choice fell on a bi-dimensional height independent spherical gaussian function.

It is worth noting that in a spherical surface the length of one degree in latitude has the same value all over the surface, while the length of one degree in longitude depends on the considered latitude. As a consequence, to take into account the Earth's spherical symmetry, we would need to calculae the length of the maximum circle between every grid point and the assimilated station. This calculation is however time-consuming and it should be done for every height (the maximum circle length over a sphere depends on the sphere's radius), this is why we chose to redefine the sigma parameter of the spherical gaussian function including in it the latitude dependence.

According to this, the considered gaussian radial basis weighting function formula is:

$$g_{ij,l} = e^{-\frac{\sigma^2 \cdot (x_i - X_{,l})^2 + \left(\frac{\sigma}{cos(Y_{,l})}\right)^2 (y_j - Y_{,l})^2}{2 \cdot \sigma^2 \cdot \left(\frac{\sigma}{cos(Y_{,l})}\right)^2}}, \quad (1)$$

where

- $x_i \in [lonini, lonfin]$ is the longitude array indexed by i, with bounds *lonini* (the initial longitude) and *lonfin* (the final longitude), and length *nlon*, dependent on the chosen step size;
- $y_j \in [latini, latfin]$ is the latitude array indexed by j, with bounds *latini* (the initial latitude) and *latfin* (the final latitude), and length *nlat*, dependent on the chosen step size;
- σ is the parameter of the gaussian function.

With this formulation, a bi-dimensional map (on the chosen grid) of the gaussian function (equal for every height), is obtained for every assimilated station. Each gaussian function has a maximum equal to 1 at the station point $(X_{,l}, Y_{,l})$, and it decreases getting away from it, according to the value of σ.

Since the assimilated profiles must be simultaneously taken into account in the assimilation procedure, while maintaining over each station electron density values as similar as possible to the assimilated ones, the weights provided by each gaussian function defined in (1) are properly normalized according to the following expression:

$$G_{ij} = \sum_{l=1}^{nstation} \left(\frac{g_{ij,l}}{\sum_l g_{ij,l}} \right). \quad (2)$$

After that, a weighted mean $(A_{ij,k})$ of the assimilated electron density values $(I_{k,l})$ is performed multiplying them by the associated gaussian map defined in (2), for each grid point and for every height, according to the following expression:

$$A_{ij,k} = \sum_{l=1}^{nstation} \left(\frac{g_{ij,l}}{\sum_l g_{ij,l}} \right) \cdot I_{l,k}. \quad (3)$$

In (3) we write $I_{l,k}$ (instead of $I_{k,l}$) because the summation is carried out on the station index l for every k height. Being this operation made for every height, a k index appears to the right of comma in A.

Concurrently, also the weight $C_{ij,k}$ of the background is calculated as follows:

$$C_{ij,k} = \sum_{l=1}^{nstation} \left(1_{ij} - \frac{g_{ij,l}}{\sum_l g_{ij,l}} \right) \cdot b_{l,k}, \quad (4)$$

where 1_{ij} is a bi-dimensional matrix made up of one, and $b_{l,k}$ are k (one for each height) one-dimensional vectors made up of background electron density values at the assimilated station grid points.

In this way, both the assimilated profiles $(I_{k,l})$ and background values $(b_{k,l})$ are weighted by the same function (G_{ij}) defined in (2). Finally, to obtain a modelled bi-dimensional electron density matrix $(M_{ij,k})$, the information derived after assimilating the vertical electron density profiles (now spread on all grid points) is merged with that given by the background reference state, as follows:

$$\begin{aligned} M_{ij,k} &= A_{ij,k} + C_{ij,k} = G_{ij} \cdot I_{k,l} + (1_{ij} - G_{ij}) \cdot b_{k,l} \\ &= B_{ij,k} + G_{ij} \cdot (I_{k,l} - b_{k,l}), \end{aligned} \quad (5)$$

where $B_{ij,k} = \sum_l 1_{ij} \cdot b_{l,k}$.

Eq. (5) tells us that the output matrix $M_{ij,k}$ consists of the summation of two parts: the background one ($B_{ij,k}$), and the difference between assimilated ($I_{k,l}$) and background ($b_{k,l}$) values, known as *Innovation*, weighted by the so called *Gain Matrix* G_{ij}. In this way, where G_{ij} tends to zero (far enough from the assimilated stations, depending on the σ value), the output smoothly tends to the background one, while near the assimilated stations the background is corrected, depending on the degree of innovation brought by the assimilated values.

3. Data analysis and results

The geographic area considered in this study is essentially the Mediterranean one (extending in latitude from 30.00°N to 44.00°N and in longitude from −7.00°W to 39.00°E). The ionospheric working stations included in this region are: El Arenosillo (37.10°N, 6.70°W, Spain), Roquetes (40.80°N, 0.50°E, Spain), Rome (41.80°N, 12.50°E, Italy), Gibilmanna (37.90°N, 14.00°E, Italy), San Vito (40.60°N, 17.80°E, Italy), Athens (38.00°N, 23.50°E, Greece), and Nicosia (35.03°N, 33.16°E, Cyprus).

In order to compare *IRIEup_re(V)* and *ISP* models consistently, it is necessary that they fulfill the same conditions; this means that both have to assimilate validated measured electron density profiles from the same reference stations, included in the Mediterranean area, and have to be tested over the same truth sites which, in the specific case, are: Athens, Nicosia, Roquetes, and San Vito.

Nevertheless, we have also applied the *IRIEup* model considering as reference stations not only those working in the Mediterranean sector, but also other European ionospheric stations (located in an area extending in latitude from 30.00°N to 60.00°N and in longitude from −15.00° W to 45.00°E, bolded in Table 1), in case corresponding autoscaled electron density profiles were available.

Specifically, as already mentioned in the introduction, the *IRIEup* model was applied for two different operational modes: (a) without taking care of validating the electron density profiles to be assimilated (*IRIEup(NV)* mode); (b) discarding in the assimilation procedure, those electron density profiles whose autoscaling was not correctly performed (*IRIEup(V)* mode).

Table 1
European ionospheric stations considered in this study; those not included in the Mediterranean sector, and used in the two operative modes *IRIEup(NV)* and *IRIEup(V)*, are bolded.

Station	Latitude	Longitude
Athens (Greece)	38.00°N	23.50°E
Chilton (United Kingdom)	51.50°N	359.40°W
Dourbes (Belgium)	50.10°N	4.60°E
El Arenosillo (Spain)	37.10°N	6.70°W
Fairford (United Kingdom)	51.70°N	358.50°W
Gibilmanna (Italy)	37.90°N	14.00°E
Juliusruh (Germany)	54.60°N	13.40°E
Moscow (Russian)	55.47°N	37.30°E
Nicosia (Cyprus)	35.03°N	33.16°E
Pruhonice (Czech Republic)	50.00°N	14.60°E
Rome (Italy)	41.80°N	12.50°E
Roquetes (Spain)	40.80°N	0.50°E
San Vito (Italy)	40.60°N	17.80°E
Warsaw (Poland)	52.20°N	21.10°E

IRIEup_re(V), *ISP*, *IRIEup_re(NV)*, and *IRIEup(V)* models provide a 3-D electron density specification of the ionosphere extending in latitude from 30.00°N to 44.00°N and in longitude from −7.00°W to 39.00°E, with a 1° × 1° degree resolution.

3-D electron density matrices are obtained also after assimilating autoscaled electron density profiles. Specifically, the Adaptive Ionospheric Profiler (AIP) (Scotto, 2009; Scotto et al., 2012), an integral part of AUTOSCALA (Scotto and Pezzopane, 2002, 2008; Pezzopane and Scotto, 2005, 2007), was applied to get measured electron density profiles from the ionograms recorded by the AIS-INGV ionosonde (Zuccheretti et al., 2003) at Rome and Gibilmanna, and also from the ionograms recorded by the VISRC2 ionosonde in Warsaw; electron density profiles measured in the other stations were instead obtained applying the ARTIST system on the ionograms recorded by the DPS4 Digisonde (Reinisch et al., 2009), which reconstructs the ionospheric bottom side profile according to the technique developed by Reinisch and Huang (1983), and gives also an estimation of the ionospheric topside profile which relies on the F2-layer peak characteristics (Reinisch and Huang, 2001). Electron density profiles autoscaled in Rome and Gibilmanna were downloaded through the electronic Space Weather upper atmosphere database (eSWua) (http://www.eswua.ingv.it/, Romano et al., 2008). The interactive ionogram scaling software, SAO Explorer, developed at the University of Massachusetts Lowell Center for Atmospheric Research (UMLCAR) (http://ulcar.uml.edu/SAO-X/SAO-X.html) (Khmyrov et al., 2008; Reinisch and Galkin, 2011), was instead used to download electron density profiles recorded in the other stations considered in this study (see Table 1).

To investigate the reliability of *IRI*, *IRIEup_re(V)*, *ISP*, *IRIEup(NV)*, and *IRIEup(V)* models during disturbed ionospheric conditions, we selected some recent geomagnetic storms occurred in March and December 2015, and October 2016. Specifically, we selected the periods 17–22 March 2015, 19–22 December 2015, and 13–14 October 2016, to be focused on periods for which the Dst geomagnetic index is below −30 nT. As it can be inferred from Fig. 1, these periods basically include the main phase of the geomagnetic storm and the first part of its recovery phase. The geomagnetic storm of 17–22 March 2015 is classified "severe", being the minimum value of Dst equal to −223 nT, while geomagnetic storms of 19–22 December 2015, and 13–14 October 2016, are classified "intense", since corresponding minimum values of Dst are equal to −155 and −104 nT respectively (Pallocchia et al., 2006).

To ensure that the chosen periods were representative of a strongly disturbed ionosphere too, *fo*F2 hourly monthly

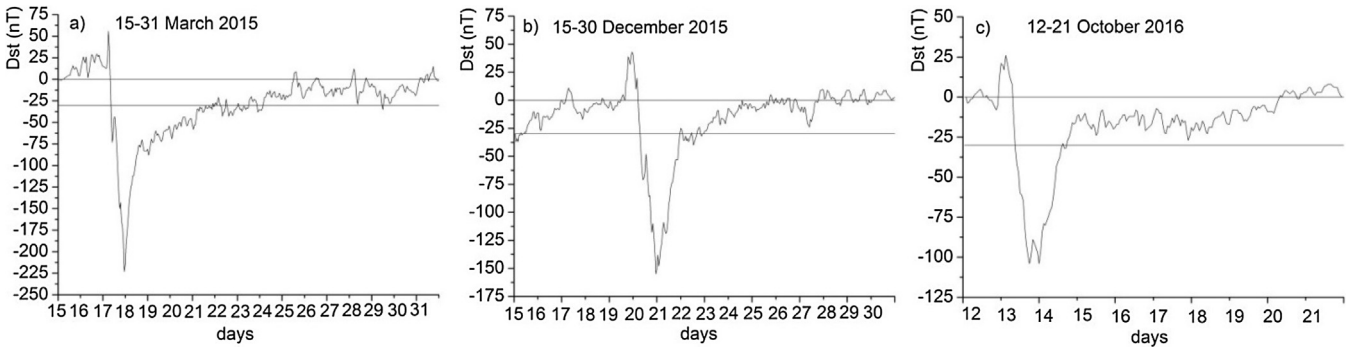

Fig. 1. Dst index recorded in the time intervals (a) 15–31 March 2015; (b) 15–30 December 2015; (c) 12–21 October 2016. Horizontal lines mark the levels 0 and −30 nT.

median values ($foF2_{med}$) calculated by the SIRM model (Zolesi et al., 1993), were compared to the *fo*F2 hourly autoscaled measurements given by ARTIST ($foF2_{meas}$) for each station included in the Mediterranean area. The reliability of *fo*F2 hourly autoscaled values was checked by the visual inspection of the corresponding ionograms (downloadable at: http://ulcar.uml.edu/DIDBase/). As an example, Fig. 2 shows the *fo*F2 monthly median trend predicted by SIRM and the autoscaled one for the period 17–22 March 2015 at Roquetes, San Vito, Athens, and Nicosia.

Cases showing differences ($foF2_{meas}$ - $foF2_{med}$) ≥ 1 MHz (positive phases) and ≤−1 MHz (negative phases) were considered significantly disturbed also from the ionospheric point of view. This criterion allowed us to select, for each station, only those epochs characterized by very disturbed ionospheric conditions. The "status" of very disturbed ionospheric condition, simultaneously occurring at least in six out of the seven Mediterranean stations considered in this study, is a further requirement aimed to guarantee that the epochs considered to test *IRIEup_re(V)*, *ISP*, *IRIEup(NV)*, and *IRIEup(V)* models, refer actually

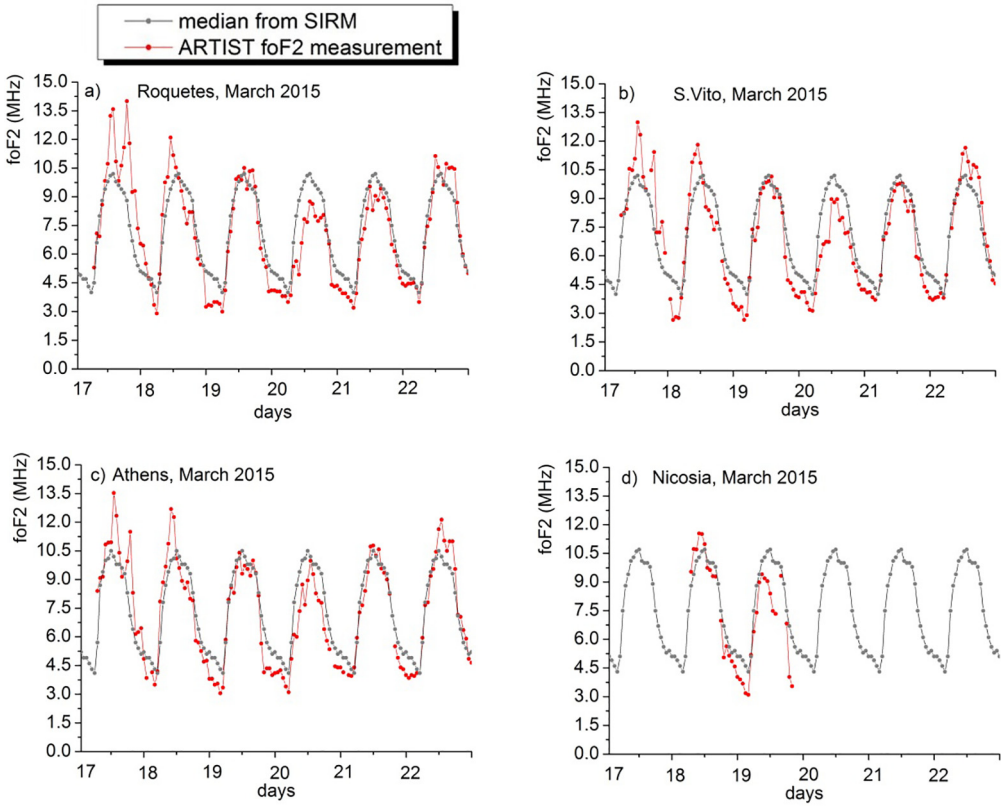

Fig. 2. (Red) hourly *fo*F2 autoscaled measurements and (grey) hourly monthly median *fo*F2 values predicted by SIRM for the period 17–22 March 2015 at (a) Roquetes, (b) San Vito, (c) Athens, and (d) Nicosia. (For interpretation of the references to colour in this figure legend, the reader is referred to the web version of this article.)

to magneto-ionospheric storm conditions involving all the Mediterranean sector. Moreover, ionograms autoscaled by ARTIST and AUTOSCALA were visually inspected and validated discarding those showing a misleading autoscaling, so that only consistent electron density profiles were assimilated by *IRIEup_re(V)*, *ISP*, and *IRIEup(V)* models. Following these criteria, several cases were rejected and only a definite number of epochs were selected. A summary picture, showing the selected epochs and different combinations of reference and truth sites is given in Fig. 3.

Finally, in order to evaluate how a "bad" ingestion of electron density profiles can affect the predictive capabilities of *IRIEup* model, the same epochs were also considered in the *IRIEup(NV)* operational mode.

As already said in the introduction, for the epochs listed in Fig. 3, measured oblique ionograms derived from radio links established within the Mediterranean area are not available. This means that a comparison between measured and synthetic oblique-incidence radiosoundings is not possible.

Nevertheless, 3-D electron density distributions of the ionosphere, calculated by the *IRI* model and assimilative *IRIEup_re(V)*, *ISP*, *IRIEup(NV)*, and *IRIEup(V)* models, were taken as input by IONORT to compute quasi-vertical ionograms at the truth sites of Roquetes, San Vito, Athens, and Nicosia, simulating some very short radio links between the truth site, considered as the transmitting station (Tx), and a location very close to Tx, considered as the receiving station (Rx). Table 2 shows the radio links for which synthesized quasi-vertical ionograms were computed by IONORT. Some examples of synthetic ionograms calculated by the IONORT-*IRI*/*IRIEup_re(V)*/*ISP*/*IRIEup(NV)*/*IRIEup(V)* system, for some of the epochs listed in Fig. 3, and corresponding ionograms recorded by the DPS4 Digisonde, are presented in Figs. 4 and 5.

Corresponding electron density profiles provided by *IRI*, *IRIEup_re(V)*, *ISP*, *IRIEup(NV)*, and *IRIEup(V)* models are depicted in Fig. 6.

The values of $foF2_{meas}$ available at the truth sites were carefully inspected to check their reliability, and then compared to the O-mode of propagation maximum usable frequencies (MUFs) obtained from the synthetic quasi-vertical ionograms. This comparison is relevant because, given the relatively small distances between Tx and Rx (see Table 2), the synthetic MUF value can be considered basically as the synthetic critical frequency ($foF2_{Syn}$) of the O-mode of propagation.

To have an idea about models accuracy, we calculated the frequency distribution of the difference $(foF2_{meas} - foF2_{Syn})$ using the following ranges (R): $(J \cdot 0.3, (J+1) \cdot 0.3] \cup [(J+1) \cdot (-0.3), J \cdot (-0.3))$ MHz, where $J = 0,1,\ldots,12$. Corresponding results are presented in the form of hystograms in Fig. 7.

The goodness of *IRI*, *IRIEup_re(V)*, *ISP*, *IRIEup(NV)*, and *IRIEup(V)* models was estimated calculating the root-mean-square error (r.m.s.e.) of each model for the single truth site, and then taking into account the truth sites all at once to calculate the following global r.m.s.e.:

$$r.m.s.e_{\text{meas-Syn}} = \sqrt{\frac{\sum_{i=1}^{N}(foF2_{\text{meas}} - foF2_{\text{Syn}})^2}{N}}, \quad (6)$$

where N represents the number of cases for which the r.m.s.e. is calculated.

The results obtained after applying Eq. (6) are shown in Table 3.

4. Discussion of results and future developments

Thanks to the applicative software tool IONORT, ingesting 3-D matrices of electron density generated by the *IRI* model and *IRIEup_re(V)*, *ISP*, *IRIEup(NV)*, and *IRIEup(V)* nowcasting models, it was possible to simulate quasi-vertical ionograms (see Figs. 4 and 5) in the Mediterranean region, which gives the possibility to evaluate the performance of each model, under very disturbed magneto-ionospheric conditions.

Specifically, the application of IONORT over the radio links Athens-Eleusi (≈18 km), Nicosia-Latsia (≈20 km), Roquetes-Bitem (≈37 km), and San Vito-Brindisi (≈28 km) allows to make pertinent comparisons between synthetic critical frequencies of the O-mode of propagation ($foF2_{Syn}$) and corresponding measurements ($foF2_{meas}$) available at the truth sites of Athens, Nicosia, Roquetes, and San Vito.

The statistical analysis of ($foF2_{meas}$ - $foF2_{Syn}$) frequency distributions (see Fig. 7), carried out to explore the level of accuracy of each model, provides the following results: a) a decreasing trend of number of cases (Nc), for R increasing from 1 to 3, values of $Nc \leq 1$ for $4 \leq R \leq 7$, and $Nc = 0$ for $R \geq 8$, are the peculiarities of *IRIEup_re(V)*, *ISP* and *IRIEup(V)*; b) an increasing trend of Nc for R increasing from 1 to 5, values of Nc remaining relatively high for $6 \leq R \leq 7$, $Nc = 1$ for $8 \leq R \leq 10$, and $Nc = 2$ for $R = 13$, are the characteristics observed for the *IRI* model; c) a decreasing trend of Nc for R increasing from 1 to 2, a value of Nc relatively high for $R = 3$, values of $Nc \leq 3$ for $4 \leq R \leq 7$, and $Nc = 1$ for $R = 11$, characterize the *IRIEup(NV)* model.

Given that high values of R define ranges for which the difference ($foF2_{meas}$ - $foF2_{Syn}$) becomes significant, the considerations made above suggest that $foF2_{Syn}$ values calculated ingesting *IRIEup_re(V)*, *ISP* and *IRIEup(V)* 3-D electron density matrices, are clearly more accurate than those obtained ingesting *IRI* and *IRIEup(NV)* ones.

This issue is also confirmed by the results (see Table 3) showing the global accuracy expressed in terms of r.m.s.e. provided by each model: 1.75, 0.88, 0.52, 0.50, and 0.44 MHz for *IRI*, *IRIEup(NV)*, *IRIEup_re(V)*, *IRIEup(V)*, and *ISP* respectively. This indicates that the global performance provided by the *IRI* model is by far

A) Epochs with 7 measurements simultaneously available

Epochs	El Are	Roq	Rom	Gib	S. Vito	Ath	Nic
19/03/2015-19:00	ART	ART	AUT	AUT	ART	ART	ART
20/12/2015-22:00	ART	ART	AUT	AUT	ART	ART	ART
20/12/2015-23:00	ART	ART	AUT	AUT	ART	ART	ART

Reference stations (5): El Arenosillo, Rome, Gibilmanna, S. Vito, Nicosia
Test sites (2): Roquetes, Athens

B) Epochs with 6 measurements simultaneously available

Epochs	El Are	Roq	Rom	Gib	S. Vito	Ath	Nic
18/03/2015-09:00*	DNA	ART	AUT	AUT	ART	ART	ART
18/03/2015-23:00	DNA	ART	AUT	AUT	ART	ART	ART
19/03/2015-00:00	DNA	ART	AUT	AUT	ART	ART	ART
19/03/2015-01:00	DNA	ART	AUT	AUT	ART	ART	ART
19/03/2015-02:00	DNA	ART	AUT	AUT	ART	ART	ART
19/03/2015-03:00	DNA	ART	AUT	AUT	ART	ART	ART
14/10/2016-07:00	DNA	ART	AUT	AUT	ART	ART	ART
14/10/2016-11:00	DNA	ART	AUT	AUT	ART	ART	ART
14/10/2016-12:00	DNA	ART	AUT	AUT	ART	ART	ART

a) Reference stations (5): Roquetes, Rome, Gibilmanna, Athens, Nicosia
Test sites (1): S. Vito * case not considered
b) Reference stations (5): Roquetes, Rome, Gibilmanna, Athens, S. Vito
Test sites (1): Nicosia

C) Epochs with 6 measurements simultaneously available

Epochs	El Are	Roq	Rom	Gib	S. Vito	Ath	Nic
17/03/2015-13:00	ART	ART	AUT	AUT	ART	ART	DNA
20/03/2015-08:00	ART	ART	AUT	AUT	ART	ART	DNA
20/03/2015-09:00	ART	ART	AUT	AUT	ART	ART	DNA
20/03/2015-10:00	ART	ART	AUT	AUT	ART	ART	DNA
20/03/2015-14:00	ART	ART	AUT	AUT	ART	ART	DNA
20/03/2015-15:00	ART	ART	AUT	AUT	ART	ART	DNA
20/03/2015-16:00	ART	ART	AUT	AUT	ART	ART	DNA
20/12/2015-20:00	ART	ART	AUT	AUT	ART	ART	DNA
20/12/2015-21:00	ART	ART	AUT	AUT	ART	ART	DNA

a) Reference stations (5): El Arenosillo, Roquetes, Rome, Gibilmanna, Athens
Test sites (1): S. Vito
b) Reference stations (5): El Arenosillo, Rome, Gibilmanna, Athens. S. Vito
Test sites (1): Roquetes

Fig. 3. Epochs considered in this study. ART and AUT indicate cases for which *fo*F2 value and electron density profiles are those autoscaled by ARTIST and AUTOSCALA respectively. DNA marks cases for which *fo*F2 autoscaled data are not available.

the worst, followed by the *IRIEup(NV)* model, while the *IRIEup_re(V)* and *IRIEup(V)* performance can be considered equivalent and slightly lower than the *ISP* one.

A more detailed analysis of the results about the accuracy provided by the different models in each single truth site, suggests other considerations:

Table 2
Radio links established to calculate synthesized quasi vertical ionograms for each epoch listed in Fig. 3. Truth sites for which *fo*F2 autoscaled measurements are available for testing are indicated in bold.

Tx-Rx	Azimuth (°)	Distance (km)
Athens (38.00°N, 23.50°E) - Eleusi (38.00°N, 23.30°E)	270.0	≈18
Nicosia (35.03°N, 33.16°E) - Latsia (35.00°N, 33.20°E)	89.9	≈20
Roquetes (40.80°N, 0.50°E) - Bitem (40.50°N, 0.30°E)	206.8	≈37
San Vito (40.60°N, 17.80°E) - Brindisi (40.40°N, 17.60°E)	217.3	≈28

(a) When comparing *IRIEup_re(V)* and *ISP* models, assimilating validated measured electron density profiles from the same reference stations we find that:
   (1) at Roquetes, *IRIEup_re(V)* performs better than *ISP* (r.m.s.e.$_{IRIEup\_re(V),Roq} = 0.43$ MHz v.s. r.m.s.e.$_{ISP,Roq} = 0.68$ MHz);
   (2) *ISP* performs slightly better than *IRIEup_re(V)* at Athens (r.m.s.e.$_{ISP,Ath} = 0.27$ MHz v.s. r.m.s.e.$_{IRIEup\_re(V),Ath} = 0.39$ MHz) and San Vito (r.m.s.e.$_{ISP,S.Vito} = 0.23$ MHz v.s. r.m.s.e.$_{IRIEup\_re(V),\ S.Vito} = 0.35$ MHz);
   (3) at Nicosia, *ISP* performs better than *IRIEup_re(V)* (r.m.s.e.$_{ISP,Nic} = 0.36$ MHz v.s. r.m.s.e.$_{IRIEup\_re(V),Nic} = 0.83$ MHz).

It is worth noting that the *ISP* procedure (Pezzopane et al., 2011, 2013) relies on the SIRMUP regional model whose validity area, extending approximately in latitude from 38.00°N to 60.00°N and in longitude from 3.50°W to 21.00°E, covers pretty well the Mediterranean sector; the operational mode *IRIEup_re(V)* is instead based only on the *IRI* model.

These considerations could explain why the *ISP* performance is overall better than the *IRIEup_re(V)* one; in fact, due to past international efforts devoted to the development and improvement of regional ionospheric modeling (Bradley, 1999; Hanbaba, 1999), it is currently recognized by the scientific community that regional models can provide, over limited areas, a representation of the ionosphere more accurate than the one that can be achieved by global models.

IRIEup_re(V) results obtained at Nicosia deserve particular attention since it is a somewhat isolated truth-site, pretty far from assimilated reference stations (≈10° in longitude away from Athens). For these conditions, the weight of assimilated vertical electron density profiles, which depends on the value of the σ parameter, can be lower than the weight due to the already updated background (calculated by IRI-SIRMUP and IRI UP procedures, respectively for ISP and IRIEup). In virtue of these considerations, the worsening of *IRIEup_re(V)* at Nicosia can be ascribed to the weakness of the IRI UP method in describing the effective indices distribution for those points pretty far from assimilated reference stations and the outer edge of the considered Mediterranean grid; in fact, in these cases there are few available stations, making it difficult to obtain a good description of the spatial correlation of the modelled quantity through the Kriging method (Kitanidis, 1997).

(b) It must be pointed out that, owing to the limited number of stations used in the operational mode *IRIEup_re(V)*, the *IRIEup* model does not exploit fully its potentiality in providing a 3-D ionospheric mapping as much as possible close to the real ionospheric conditions. For this reason, we have also applied the *IRIEup* model considering the operational modes *IRIEup(NV)* and *IRIEup(V)* including additional European stations for which ARTIST autoscaled electron density profiles were available, besides the ones in the Mediterranean sector. In this way, the use of a larger number of available reference stations, over an extended geographical area, allowed us to obtain an improved empirical variogram, which is necessary to properly describe the spatial correlation of effective indices through the Kriging method (Kitanidis, 1997; Pignalberi et al., 2018a,b).

Comparing *IRIEup_re(V)*, *IRIEup(NV)* and *IRIEup(V)* models, the last two assimilating not validated and validated measured electron density profiles from all reference stations listed in Table 1, we find that:

(1) at Athens, Nicosia, Roquetes, and San Vito, *IRIEup(NV)* (r.m.s.e.$_{IRIEup(NV),Ath} = 1.30$ MHz; r.m.s.e.$_{IRIEup(NV),Nic} = 1.36$ MHz; r.m.s.e.$_{IRIEup(NV),Roq} = 0.84$ MHz; r.m.s.e.$_{IRIEup(NV),S.Vito} = 0.33$ MHz) performs much worse than *IRIEup_re(V)* (r.m.s.e.$_{IRIEup\_re(V),Ath} = 0.39$ MHz; r.m.s.e.$_{IRIEup\_re(V),Nic} = 0.83$ MHz; r.m.s.e.$_{IRIEup\_re(V),Roq} = 0.43$ MHz; r.m.s.e.$_{IRIEup\_re(V),S.Vito} = 0.35$ MHz) and *IRIEup(V)* (r.m.s.e.$_{IRIEup(V),Ath} = 0.05$ MHz; r.m.s.e.$_{IRIEup(V),Nic} = 0.85$ MHz; r.m.s.e.$_{IRIEup(V),Roq} = 0.44$ MHz; r.m.s.e.$_{IRIEup(V),S.Vito} = 0.29$ MHz); these results demonstrate how the assimilation of correct electron density profiles is of utmost importance for obtaining a most reliable ionospheric modeling;
(2) While at Nicosia and Roquetes *IRIEup_re(V)* and *IRIEup(V)* performance can be considered practically equivalent (r.m.s.e.$_{IRIEup\_re(V),Nic} = 0.83$ MHz v.s. r.m.s.e.$_{IRIEup(V),Nic} = 0.85$ MHz; r.m.s.e.$_{IRIEup\_re(V),Roq} = 0.43$ MHz v.s. r.m.s.e.$_{IRIEup(V),Roq} = 0.44$ MHz), at San Vito *IRIEup(V)* performs slightly

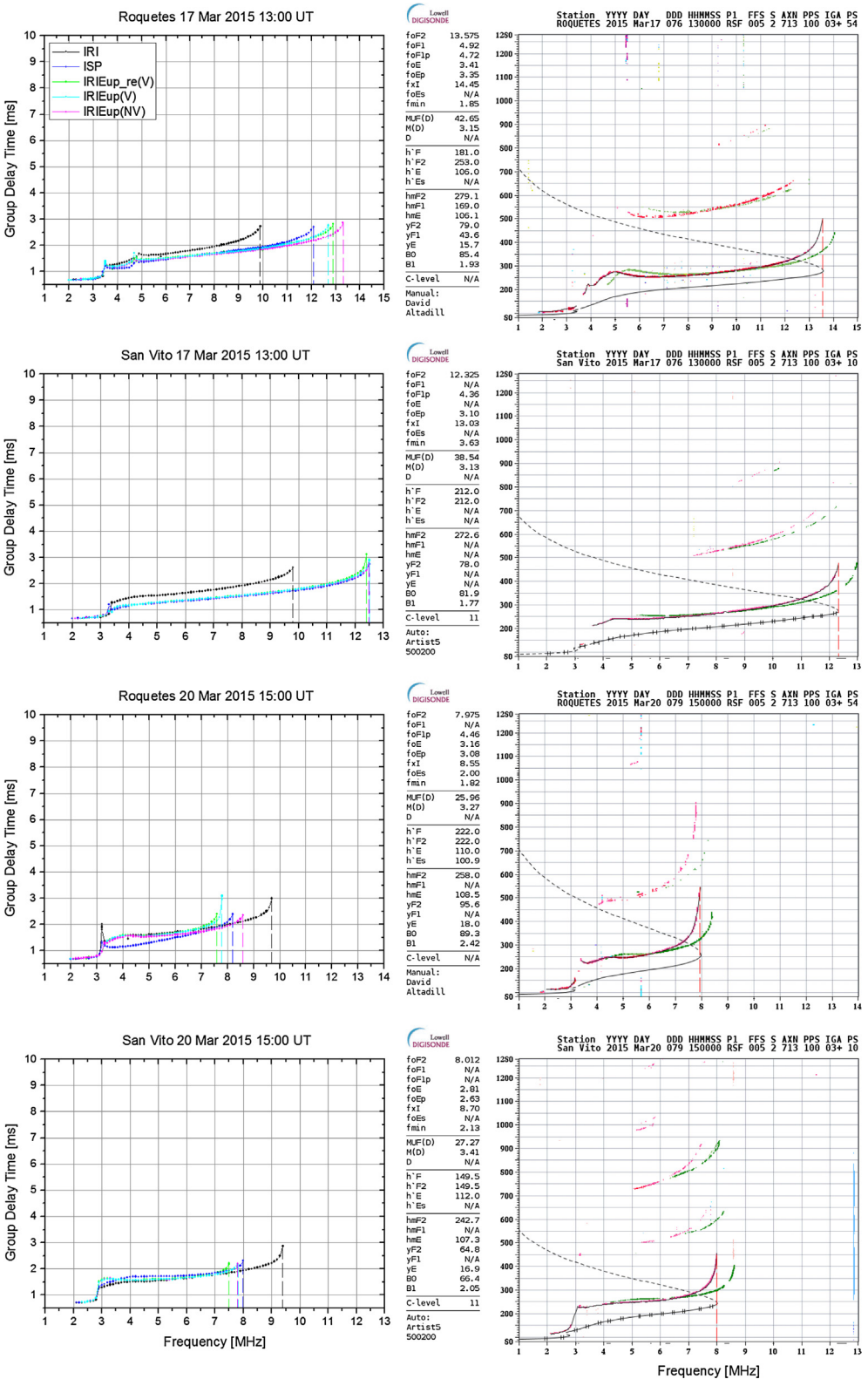

Fig. 4. (Left) synthetic ionograms and (right) measured ionograms for some of the epochs listed in Fig. 3. Vertical dashed lines highlight *fo*F2 values.

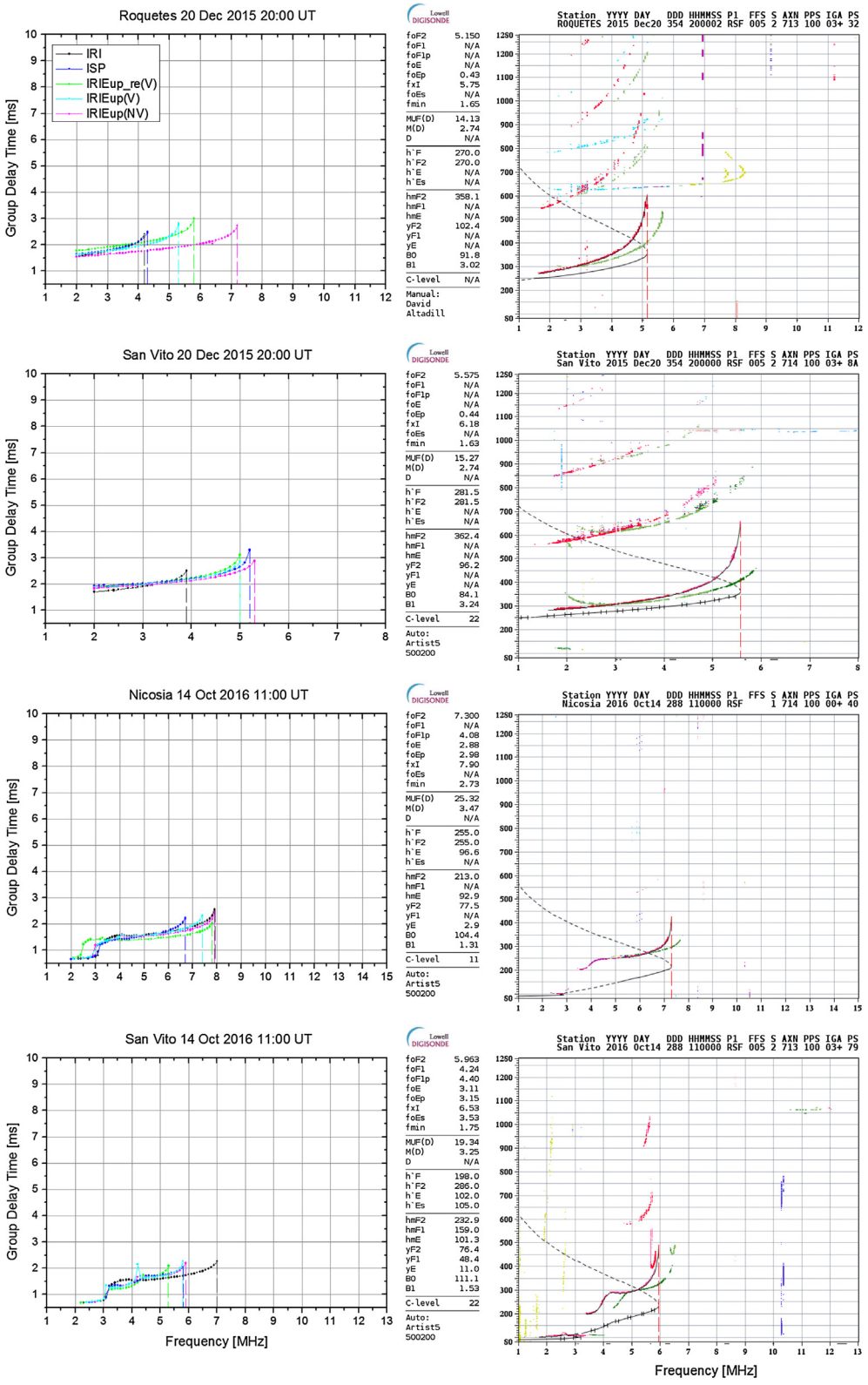

Fig. 5. Same as Fig. 4.

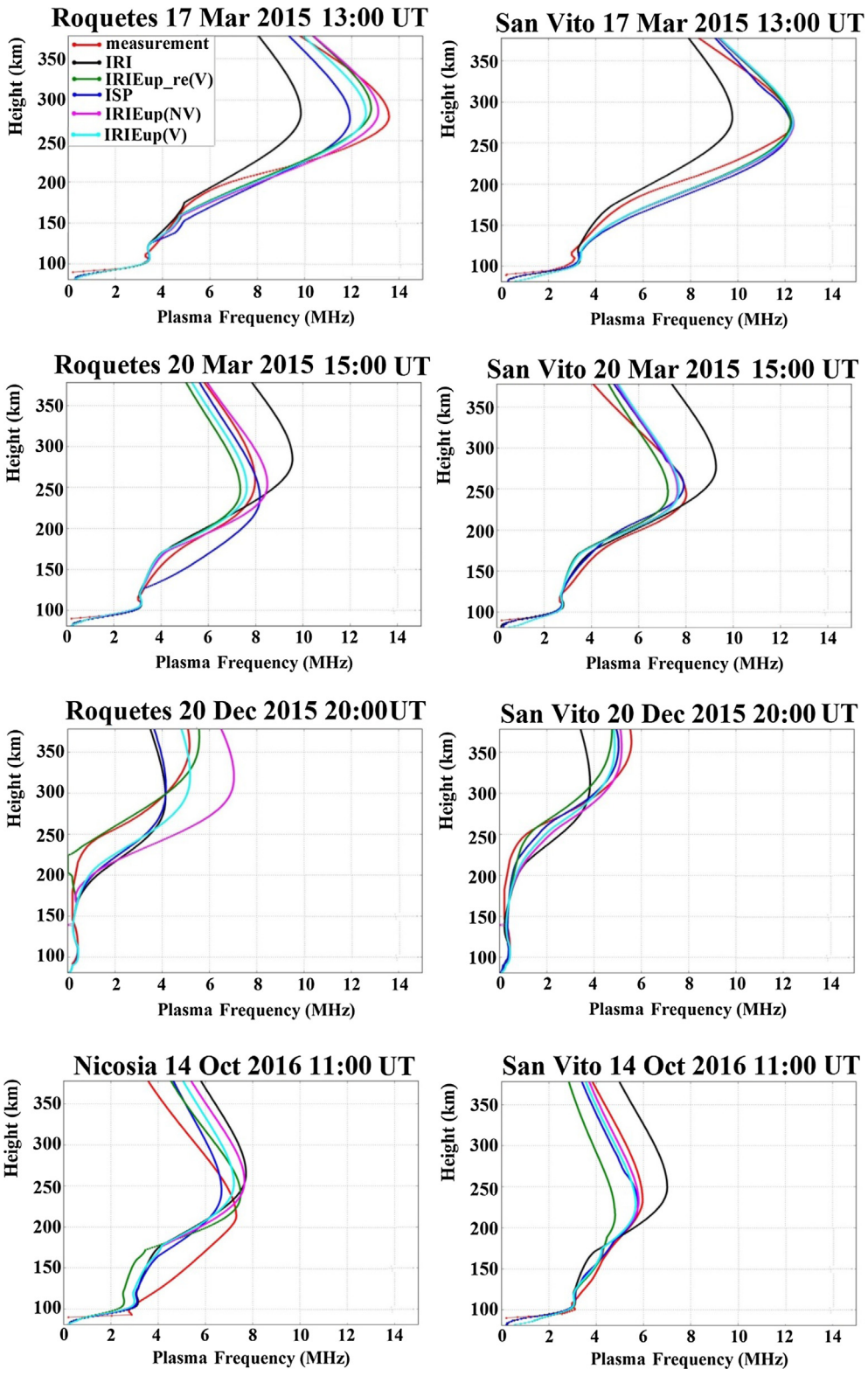

Fig. 6. Electron density profiles for the same epochs considered in Figs. 4 and 5.

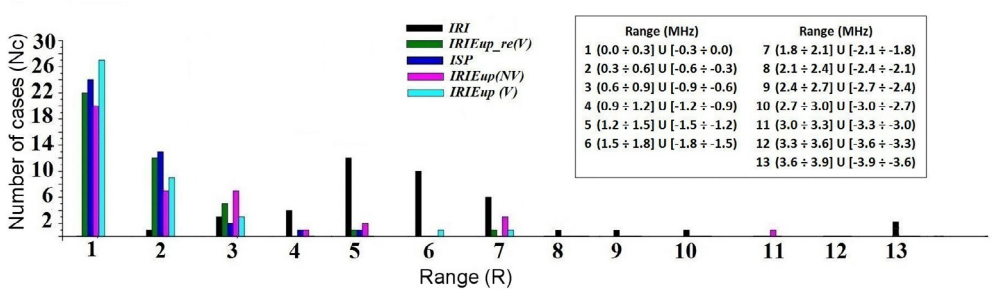

Fig. 7. Comparison between *IRI*, *IRIEup_re(V)*, *ISP*, *IRIEup(NV)*, and *IRIEup(V)* hystograms in terms of ($foF2_{meas}$-$foF2_{Syn}$). The meaning of the abscissa is reported in the upper right part of the panel.

Table 3
IRI, *IRIEup_re(V)*, *ISP*, *IRIEup(NV)*, and *IRIEup(V)* r.m.s.e. (MHz).

Test Sites	*IRI*	*IRIup_re(V)*	*ISP*	*IRIEup(NV)*	*IRIEup(V)*	N
Athens	1.97	0.39	0.27	1.30	0.05	3
Nicosia	1.45	0.83	0.36	1.36	0.85	9
Roquetes	2.03	0.43	0.68	0.84	0.44	12
San Vito	1.64	0.35	0.23	0.33	0.29	17
Global	1.75	0.52	0.44	0.88	0.50	41

better than *IRIEup_re(V)* (r.m.s.e.$_{IRIEup(V),S.Vito}$ = 0.29 MHz v.s. r.m.s.e.$_{IRIEup\_re(V),S.\ Vito}$ = 0.35 MHz), while a significant improvement is obtained at Athens (r.m.s.e.$_{IRIEup(V),Ath}$ = 0.05 MHz v.s. r.m.s.e.$_{IRIEup\_re(V),Ath}$ = 0.39 MHz).

These outcomes highlight that the larger is the number of reference stations, from which the electron density profiles are assimilated, the more *IRIEup* algorithm works at best of its possibilities.

(c) When comparing *ISP* with *IRIEup(V)*, we find that:
  (1) at Roquetes, *IRIEup(V)* performs better than *ISP* (r.m.s.e.$_{IRIEup(V),Roq}$ = 0.44 MHz v.s. r.m.s.e.$_{ISP,Roq}$ = 0.68 MHz), but a particular improvement respect to *IRIEup_re(V)* is not observed (r.m.s.e.$_{IRIEup\_re(V),Roq}$ = 0.43 MHz);
  (2) at Athens, *IRIEup(V)* performs better than *ISP* (r.m.s.e.$_{IRIEup(V),Ath}$ = 0.05 MHz v.s. r.m.s.e. $_{ISP,Ath}$ = 0.27 MHz) and a significant improvement is also observed respect to *IRIEup_re(V)* (r.m.s.e.$_{IRIEup\_re(V),Ath}$ = 0.39 MHz);
  (3) at San Vito, although *IRIEup(V)* shows slightly better results than *IRIEup_re(V)* (r.m.s.e.$_{IRIEup(V),S.Vito}$ = 0.29 MHz v.s. r.m.s.e. $_{IRIEup\_re(V),\ S.Vito}$ = 0.35 MHz), *ISP* continues to perform better (r.m.s.e.$_{ISP,S.Vito}$ = 0.23 MHz);
  (4) at Nicosia, *ISP* performance continues to be better (r.m.s.e.$_{ISP,Nic}$ = 0.36 MHz v.s. r.m.s.e. $_{IRIEup(V),Nic}$ = 0.85 MHz) because *IRIEup(V)* does not show any improvement with respect to *IRIEup_re(V)* (r.m.s.e.$_{IRIEup\_re(V),Nic}$ = 0.83 MHz).

It must be pointed out that these results come out from a non-peer to peer comparison between *ISP* and *IRIEup (V)*, since the autoscaled data assimilated did not come from exactly the same reference stations. Notwithstanding the overall improvement of *IRIEup(V)* respect to *IRIEup_re(V)*, mainly due to its capabilities to produce a more accurate ionospheric representation over Athens, *ISP* performance globally continues to be better than the *IRIEup(V)* one. The major accuracy of *ISP* is probably due to the regional model SIRMUP underlying the *ISP* algorithm which provides a more realistic representation of the ionosphere in the Mediterranean area than the one given by the *IRI* model underlying the *IRIEup* procedure.

(d) From the comparison between the *IRI* background model and nowcasting models we find that:
  (1) at Athens, Nicosia, Roquetes, and San Vito, the *IRI* performance is considerably the worst; in fact, values of r.m.s.e. calculated for the *IRI* model at Athens (r.m.s.e$_{IRI,Ath}$ = 1.97 MHz), Nicosia (r.m.s.e$_{IRI,Nic}$ = 1.45 MHz), Roquetes (r.m.s.e$_{IRI,Roq}$ = 2.03 MHz), and San Vito (r.m.s.e$_{IRI,s.Vito}$ = 1.64 MHz) are always greater than 1.4 MHz, while those referring to *IRIEup_re(V)*, *ISP*, and *IRIEup(V)* nowcasting models are at most around 0.8 MHz;
  (2) it is worth noting that also *IRIEup(NV)*, although it works assimilating not validated electron density profiles, can perform better than *IRI* at all truth sites. This is also testified from the comparison between the magenta (*IRIEup(NV)*) and black (*IRI*) electron density profiles, and the measured electron density profiles shown in red in Fig. 6.

These outcomes show unequivocally that the *IRI* model does not adequately "capture" the geomagnetic-ionospheric storm effects occurring over a relatively large area. On the contrary, the availability of autoscaled and validated data, allows nowcasting models to "reproduce" the storm effects impacting the ionosphere and hence to get a 3-D ionospheric image more accurate than that provided by the *IRI* model. This conclusion looks much more noticeable by comparing the electron density profiles shown in Fig. 6.

It should be noted that the results, achieved comparing $foF2_{meas}$ with $foF2_{Syn}$ at the truth sites, reflect indirectly how much realistic the 3-D electron density ionospheric distributions generated by the *IRI* background model and nowcasting models are, in representing the ionosphere behaviour during geomagnetic-ionospheric storm conditions like those considered in this study.

ISP results constitute a further confirmation of good capabilities of the *ISP* procedure, already proved in some recent works (Pezzopane et al., 2011, 2013; Settimi et al., 2013, 2015; Pietrella et al., 2016), in providing a reliable 3-D mapping of the ionosphere.

Nevertheless, the *ISP* algorithm relies on the SIRMUP regional model and consequently its applicability is limited to the Mediterranean region. On the contrary, the *IRIEup* algorithm can be potentially applied to any region characterized by a network of ionosondes. This greatly compensates its slightly lower performance when compared to *ISP*. Another benefit of the *IRIEup* algorithm is a computer run time lower than that of the *ISP* one.

With regard to future developments, both an appropriate modification of the source code describing the *ISP* assimilation procedure, and a rearrangemnet of the IONORT source code, are in progress to reduce the computer run time of the *IONORT-ISP* system, so as to speed the corresponding 3-D ionospheric mapping and ray tracing over the European region.

Lastly, MUF measurements, from oblique-incidence ionospheric radiosoundings recorded anywhere in the world, could be exploited to investigate the behaviour of the *IONORT-IRIEup* system also out of the European area and under different helio-geophysical conditions.

5. Summary

A comparative study of some assimilative ionospheric models during some intense and severe geomagnetic-ionospheric storms has been carried out. Concerning the overall performance, all considered models proved to be considerably more reliable than the climatological *IRI* model. Specifically, *ISP* and *IRIEup(V)* models provided the best performance, with the former being slightly better.

The study highlighted the following two main issues:

(1) When relying on autoscaled data, you should be careful. The study in fact pointed out that outputs of *IRIEup(V)* and *IRIEup(NV)* are really different. This means that assimilative ionospheric models are powerful tools, but at the same time autoscaled data have to be properly treated/filtered before being assimilated. This is one of the next steps that will characterize the future development of *IRIEup*;

(2) Although global models represent a valuable input for a 3-D mapping of the ionosphere, regional models are a significant complement to characterize those features that are often not reproduced by global models. The study in fact pointed out that the *SIRMUP* regional model represents a valid help for the *ISP* procedure.

Acknowledgements

This publication uses data from 12 ionospheric observatories in Europe, made available via the public access portal of the Digital Ionogram Database of the Global Ionosphere Radio Observatory in Lowell, MA. The authors are indebted to the observatory directors and ionosonde operators for heavy investments of their time, effort, expertise, and funds needed to acquire and provide measurement data to academic research. The authors would also to thank the unknown referees for their comments and suggestions which have contributed to improve this paper.

References

Angling, M.J., Khattatov, B., 2006. Comparative study of two assimilative models of the ionosphere. Radio Sci. 41. https://doi.org/10.1029/2005RS003372.

Araujo-Pradere, E.A., Fuller-Rowel, T.J., Codrescu, M.V., 2002. STORM: an empirical storm-time ionospheric correction model 1. Model description. Radio Sci. 37 (5). https://doi.org/10.1029/2001RS002467.

Azzarone, A., Bianchi, C., Pezzopane, M., Pietrella, M., Scotto, C., Settimi, A., 2012. IONORT: a Windows software tool to calculate the HF ray tracing in the ionosphere. Comp. Geosc. 42, 57–63. https://doi.org/10.1016/j.cageo.2012.02.008.

Bailey, G.J., Balan, N., 1996. A low-latitude ionosphere-plasmasphere model. In: Schunk, R.W. (Ed.), STEP Handbook on Ionospheric Models. Utah State Univ, Logan, pp. 173–206.

Bamford, R.A., Stamper, R., Cander, L.R., 2008. A comparison between the hourly autoscaled and manually scaled characteristics from the Chilton ionosonde from 1996 to 2004. Radio Sci. 43 (1). https://doi.org/10.1029/2005RS003401.

Bilitza, D., 2001. International reference ionosphere 2000. Radio Sci. 36, 261–275. https://doi.org/10.1029/2000RS002432.

Bilitza, D., Reinisch, B.W., 2008. International Reference Ionosphere 2007: improvements and new parameters. Adv. Space Res. 42 (7), 599–609. https://doi.org/10.1016/j.asr.2007.07.048.

Bilitza, D., Altadill, D., Zhang, Y., Mertens, C., Truhlik, V., Richards, P., McKinnell, L.-A., Reinisch, B., 2014. The International reference ionosphere 2012 – a model of international collaboration. J. Space Weather Space Climate 4, A07. https://doi.org/10.1051/swsc/2014004.

Bilitza, D., Altadill, D., Truhlik, V., Shubin, V., Galkin, I., Reinisch, B., Huang, X., 2017. International Reference Ionosphere 2016: from ionospheric climate to real-time weather predictions. Space Weather 15 (2), 418–429. https://doi.org/10.1002/2016SW001593.

Bradley, P., 1999. PRIME (Prediction and Retrospective Ionospheric Modelling over Europe), Cost Action 238. Final Report, Rutherford Appleton Laboratory, Chilton Didcot, UK.

Buresova, D., Nava, B., Galkin, I., Angling, M., Stankov, S.M., Coisson, P., 2009. Data ingestion and assimilation in ionospheric models. Ann. Geophys. 52. https://doi.org/10.4401/ag-4575.

Daniell, R.E., Brown, L.D., Anderson, D.N., Fox, M.W., Doherty, P.H., Decker, D.T., Sojka, J.J., Schunk, R.W., 1995. Parameterized ionospheric model: a global ionospheric parameterization based on first principles models. Radio Sci. 30, 1499–1510. https://doi.org/10.1029/95RS01826.

Fuller-Rowell, T.J., Rees, D., Quegan, S., Moffett, R.J., Codrescu, M.V., Millward, G.H., 1996. A coupled thermo-sphere ionosphere model (CTIM). In: Schunk, R.W. (Ed.), STEP Handbook on Ionospheric Models. Utah State Univ, Logan, pp. 217–224.

Fuller-Rowell, T.J., Codrescu, M.V., Araujo-Pradere, E., Kutiev, I., 1998. Progress in developing a storm-time ionospheric correction model. Adv. Space Res. 22 (6), 821–827.

Galkin, I.A., Reinisch, B.W., 2008. The new ARTIST 5 for all digisondes, in ionosonde network advisory group bulletin. In: IPS Radio and Space Serv., Surry Hills, N.S.W., Australia, vol. 69, pp. 1–8. Available also at: <http://www.ips.gov.au/IPSHosted/INAG/web-69/2008/artist5-inag.pdf>.

Galkin, I.A., Reinisch, B.W., Huang, X., Bilitza, D., 2012. Assimilation of GIRO data into a real-time IRI. Radio Sci. 47. https://doi.org/10.1029/2011RS004952.

Hanbaba, R., 1999. Improved Quality of Services Ionospheric Telecommunication Systems Planning and Operation, Cost Action 251. Final Report. Published by Space Research Centre, Warsaw, Poland.

Houminer, Z., Bennett, J.A., Dyson, P.L., 1993. Real-time ionospheric model updating. J. Electr. Electr. Eng., Australia, IE Australia & IREE Australia 13 (2), 99–104.

Hochegger, G., Nava, B., Radicella, S.M., Leitinger, R., 2000. A family of ionospheric models for different uses. Phys. Chem. Earth, Part C: Solar, Terrest. Planet. Sci. 25 (4), 307–310. https://doi.org/10.1016/S1464-1917(00)00022-2.

Kitanidis, P.K., 1997. Introduction to Geostatistics: Application to Hydrogeology. Cambridge University Press.

Khmyrov, G.M., Galkin, I.A., Kozlov, A.V., et al., 2008. Exploring digisonde ionogram data with SAO-X and DIDBase. In: Proceedings of AIP Conference Radio Sounding and Plasma Physics, vol. 974, pp. 175–185. https://doi.org/10.1063/1.2885027.

Liu, R.Y., Smith, P.A., King, J.W., 1983. A new solar index which leads to improved foF2 predictions using the CCIR Atlas. Telecommun. J. 50, 408–414.

Millward, G., Moffett, R.J., Quegan, S., Fuller-Rowell, T.J., 1996. A coupled thermosphere-ionosphere-plasmasphere model (CTIP). In: Schunk, R.W. (Ed.), STEP Handbook on Ionospheric Models. Utah State Univ, Logan, pp. 239–279.

Moldwin, M., 2008. An Introduction to Space Weather. Cambridge University Press, Cambridge, 10.1017/CBO9780511801365.

Nava, B., Radicella, S.M., Azpilicueta, F., 2011. Data ingestion into NeQuick 2. Radio Sci. 46 (6). https://doi.org/10.1029/2010RS004635.

Norman, R.J., Cannon, P.S., 1997. A two dimensional analytical ray tracing technique accommodating horizontal gradients. Radio Sci. 32, 387–396. https://doi.org/10.1029/96RS03200.

Pallocchia, G., Amata, E., Consolini, G., Marcucci, M.F., Bertello, I., 2006. Geomagnetic Dst index forecast based on IMF data only. Ann. Geophys. 24 (3), 989–999, hal-00318011.

Pezzopane, M., Scotto, C., 2005. The INGV software for the automatic scaling of foF2 and MUF(3000)F2 from ionograms: a performance comparison with ARTIST 4.01 from Rome data. J. Atmos. Solar-Terr. Phys. 67 (12), 1063–1073. https://doi.org/10.1016/j.jastp.2005.02.022.

Pezzopane, M., Scotto, C., 2007. The automatic scaling of critical frequency foF2 and MUF(3000)F2: a comparison between Autoscala and ARTIST 4.5 on Rome data. Radio Sci. 42. https://doi.org/10.1029/2006RS003581.

Pezzopane, M., Pietrella, M., Pignatelli, A., Zolesi, B., Cander, L.R., 2011. Assimilation of autoscaled data and regional and local ionospheric models as input sources for real-time 3-D international reference ionosphere modeling. Radio Sci. 46, 5009. https://doi.org/10.1029/2011RS004697.

Pezzopane, M., Pietrella, M., Pignatelli, A., Zolesi, B., Cander, L.R., 2013. Testing the three-dimensional IRI-SIRMUP-P mapping of the ionosphere for disturbed periods. Adv. Space Res. 52 (10), 1726–1736. https://doi.org/10.1016/j.asr.2012.11.028.

Pietrella, M., Pezzopane, M., Settimi, A., 2016. Ionospheric response under the influence of the solar eclipse occurred on 20 March 2015: Importance of autoscaled data and their assimilation for obtaining a reliable modeling of the ionosphere. J. Atmos. Solar-Terrestr. Phys. 146, 49–57. https://doi.org/10.1016/j.jastp.2016.05.006.

Pignalberi, A., Pezzopane, M., Rizzi, R., Galkin, I., 2018a. Effective solar indices for ionospheric modeling: a review and a proposal for a real-time regional IRI. Surv. Geophys. https://doi.org/10.1007/s10712-017-9438-y.

Pignalberi, A., Pezzopane, M., Rizzi, R., Galkin, I., 2018b. Correction to: effective solar indices for ionospheric modeling: a review and a proposal for a real-time regional IRI. Surv. Geophys. 39, 169. https://doi.org/10.1007/s10712-017-9453-z.

Radicella, S.M., Leitinger, R., 2001. The evolution of the DGR approach to model electron density profiles. Adv. Space Res. 27 (1), 35–40. https://doi.org/10.1016/S0273-1177(00)00138-1.

Reinisch, B.W., Huang, X., 1983. Automatic calculation of electron density profiles from digital ionograms: 3. Processing of bottom side ionograms. Radio Sci. 18 (3), 477–492. https://doi.org/10.1029/RS018i003p00477.

Reinisch, B.W., Huang, X., 2001. Deducing topside profiles and total electron content from bottomside ionograms. Adv. Space Res. 27 (1), 23–30. https://doi.org/10.1016/S0273-1177(00)00136-8.

Reinisch, B.W., Huang, X., Galkin, I.A., Paznukhov, V., Kozlov, A., 2005. Recent advances in real-time analysis of ionograms and ionospheric drift measurements with digisondes. J. Atmos. Solar-Terr. Phys. 67 (12), 1054–1062. https://doi.org/10.1016/j.jastp. 2005.01.009.

Reinisch, B.W., Galkin, I.A., Khmyrov, G.M., et al., 2009. New Digisonde for research and monitoring applications. Radio Sci. 44 (1). https://doi.org/10.1029/2008RS004115.

Reinisch, B.W., Galkin, I.A., 2011. Global ionospheric radio observatory (GIRO). Earth Planets Space 63, 377–381.

Romano, V., Pau, S., Pezzopane, M., Zuccheretti, E., Zolesi, B., De Franceschi, G., Locatelli, S., 2008. The electronic Space Weather upper atmosphere (eSWua) project at INGV: advancements and state of the art. Ann. Geophys. 26, 345–351. https://doi.org/10.5194/angeo-26-345-2008.

Schunk, R.W. et al., 2004. Global assimilation of ionospheric measurements (GAIM). Radio Sci. 39. https://doi.org/10.1029/2002RS002794.

Scotto, C., Pezzopane, M., 2002. A software for automatic scaling of foF2 and MUF(3000)F2 from ionograms. In: Proceedings of the XXVII General Assembly of the International Union of Radio Science, 17–24 August, Maastricht, The Netherlands. International Union of Radio Science, Ghent, CD-ROM.

Scotto, C., Pezzopane, M., 2008. Removing multiple reflections from the F2 layer to improve Autoscala performance. J. Atmos. Sol. Terr. Phys. 70 (15), 1929–1934. https://doi.org/10.1016/j.jastp.2008.05.012.

Scotto, C., 2009. Electron density profile calculation technique for autoscala ionogram analysis. Adv. Space Res. 44, 756–766. https://doi.org/10.1016/j.asr.2009.04.037.

Scotto, C., Pezzopane, M., Zolesi, B., 2012. Estimating the vertical electron density profile from an ionogram: on the passage from true to virtual heights via the target function method. Radio Sci. 47. https://doi.org/10.1029/2011RS004833.

Settimi, A., Pezzopane, M., Pietrella, M., Bianchi, C., Scotto, C., Zuccheretti, E., Makris, J., 2013. Testing the IONORT-ISP system: a comparison between synthesized and measured oblique ionograms. Radio Sci. 48 (2), 167–179. https://doi.org/10.1002/rds.20018.

Settimi, A., Pietrella, M., Pezzopane, M., Bianchi, C., 2015. The IONORT-ISP-WC system: inclusion of an electron collision frequency model for the D-layer. Adv. Space Res. 55 (8), 2114–2123. https://doi.org/10.1016/j.asr.2014.07.040.

Stankov, S.M., Jodogne, J.C., Kutiev, I., Stegen, k., Warnant, R., 2012. Evaluation of automatic ionogram scaling for use in real-time ionospheric density profile specification: dourbes DGS-256/ARTIST-4 performance. Ann. Geophys. 55 (2), 283–291. https://doi.org/10.4401/ag-4976.

Tsagouri, I., Zolesi, B., Belehaki, A., Cander, L.R., 2005. Evaluation of the performance of the real-time updated simplified ionospheric regional model for the European area. J. Atm. Sol. Terr. Phys. 67 (12), 1137–1146. https://doi.org/10.1016/j.jastp.2005.01.012.

Zolesi, B., Cander, L.R., De Franceschi, G., 1993. Simplified ionospheric regional model for telecommunication applications. Radio Sci. 28 (4), 603–612. https://doi.org/10.1029/93RS00276.

Zolesi, B., Belehaki, A., Tsagouri, I., Cander, L.R., 2004. Real-time updating of the simplified ionospheric regional model for operational applications. Radio Sci. 39 (2). https://doi.org/10.1029/2003RS002936.

Zuccheretti, E., Tutone, G., Sciacca, U., Bianchi, C., Arokiasamy, B.J., 2003. The new AIS-INGV digital ionosonde. Ann. Geophys. 46 (4), 647–659. https://doi.org/10.4401/ag-4377.

Wang, C., Hajj, G., Pi, X., Rosen, I.G., Wilson, B., 2004. Development of the global assimilative ionospheric model. Radio Sci. 39. https://doi.org/10.1029/2002RS002854.